Nanoscale

Accepted Manuscript

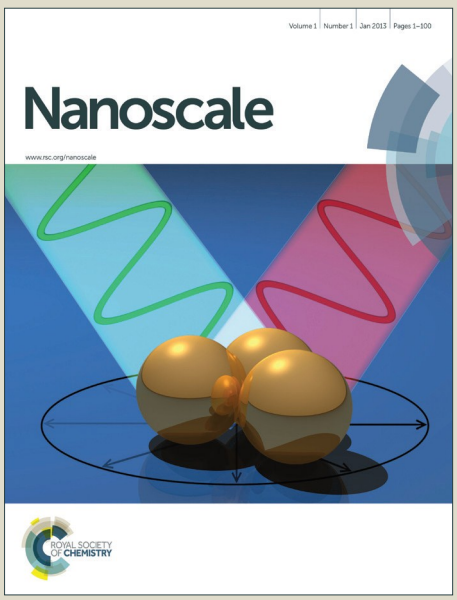

This is an *Accepted Manuscript*, which has been through the Royal Society of Chemistry peer review process and has been accepted for publication.

Accepted Manuscripts are published online shortly after acceptance, before technical editing, formatting and proof reading. Using this free service, authors can make their results available to the community, in citable form, before we publish the edited article. We will replace this *Accepted Manuscript* with the edited and formatted *Advance Article* as soon as it is available.

You can find more information about *Accepted Manuscripts* in the Information for Authors.

Please note that technical editing may introduce minor changes to the text and/or graphics, which may alter content. The journal's standard Terms & Conditions and the Ethical guidelines still apply. In no event shall the Royal Society of Chemistry be held responsible for any errors or omissions in this *Accepted Manuscript* or any consequences arising from the use of any information it contains.

ROYAL SOCIETY OF CHEMISTRY

www.rsc.org/nanoscale

Complete Voltage Recovery in Quantum Dot Solar Cells due to Suppression of Electron Capture

A. Varghese[1], M. Yakimov[1], V. Tokranov[1], V. Mitin[2], K. Sablon[3], A. Sergeev[3], and S. Oktyabrsky[1]

[1]SUNY Polytechnic Institute, Albany, NY, 12203
[2] University at Buffalo - SUNY, Buffalo, NY 14260
[3] U.S. Army Research Laboratory, Adelphi, MD 20783, USA

Extensive investigations of recent years show that an addition of quantum dots (QDs) to a single-junction solar cell decreases the open circuit voltage, V_{OC}, with respect to the reference cell without QDs. Despite numerous efforts, the complete voltage recovery in QD cells has been demonstrated only at low temperatures. To minimize the V_{OC} reduction, we propose and investigate a new approach that combines nanoscale engineering of band structure and potential profile. Our studies of GaAs solar cells with various InAs QD media demonstrate that the main cause of the V_{OC} reduction is the fast capture of photoelectrons from the GaAs conduction band (CB) to localized states in QDs. As the photoelectron capture into QDs is mainly realized via the wetting layers (WLs), we substantially reduced the WLs using two monolayer AlAs capping of QDs. In the structures with reduced WLs, the direct CB-to-QD capture is further suppressed due to charging of QDs via doping of the interdot space. The QD devices with suppressed photoelectron capture show the same V_{OC} as the GaAs reference cell together with some improvements in the short circuit current.

I. Introduction

Intriguing possibilities for nanoscale engineering of energy transfer between photons, electrons, and phonons have inspired numerous investigations of quantum dot (QD) structures for photovoltaic conversion of solar radiation.[1] It has been found that QDs may increase the conversion efficiency due to enhanced coupling with solar radiation,[2,3] multiple exciton generation,[4-6] two-step light absorption,[7-13] and thermionic emission from dots induced by hot photoelectrons.[14-16] Significant efforts in QD photovoltaics were devoted to development of the intermediate band (IB) solar cells, where hybridization of QD levels forms the intermediate band (IB), which is expected to provide two-step absorption of sub-bandgap photons, but do not introduce significant nonradiative relaxation from conduction band (CB) to QDs.[7]

Various colloidal and solid-state QD photovoltaic materials were experimentally studied. The most detailed investigations were carried out on epitaxial InAs/GaAs structures because of maturity of the growth process and well-understood properties of the III –V semiconductors.[17] Numerous data have shown that the QD medium placed in the p-n junctions may noticeably increase the short circuit current, J_{SC}, but reduces the open circuit voltage, V_{OC}.[8-11,13] Commonly, the increase of J_{SC} may be achieved by decreasing the bandgap in a traditional single-gap solar cell, and this increase is accompanied by a

Nanoscale Accepted Manuscript

reduction of V_{OC}. Recent research associates the J_{SC} increase and V_{OC} reduction in QD devices with slow radiative and fast thermal excitations of electrons from QDs to CB in InAs/GaAs structures[8-11,18,19] and similarly excitation of holes from QDs to the valence band in Ge/Si structures.[20] It is well understood now that the fast QD-to-CB excitation occurs due to the field-induced tunneling via thermo-excited QD states.[8] To suppress this process, the QD structures with relatively thick (50 -120 nm) spacer layers between QD planes were proposed, fabricated and studied.[8,11,18-20] Some improvements in output voltage were reported and discussed mainly in terms of IB kinetics.[18-22] However, the spacer layers with thickness above 30 nm prevent the IB formation, suppress electron transfer between QDs, and facilitate charge accumulation in QDs. Charged dots drastically alter kinetic and transport processes in photovoltaic devices.[23]

Charging of QDs is an efficient tool to control the microscale potential profile via selective doping and to manage QD processes via 3D nanoscale potential profile, which is formed by the barriers around dots.[14,23-25] The microscale control allows for fabrication of PV structures with sharp junctions, which improve electron-hole separation and reduce Shockley-Read-Hall recombination in the junction area. The 3D nanoscale profile is a new paradigm, which allows for efficient control of all electron kinetic and transport processes in QD media. In particular, charging of QDs via modulation n-doping of the interdot space prevents photoelectron capture into QDs.[14,23]

Returning to the problem of V_{OC} reduction, let us note that the fast thermo-activated escape from QDs results in a V_{OC} value below that of the ideal two-step absorption model.[7] However, this process does not dissipate any solar energy and cannot deteriorate the device performance with respect to the reference cell. Moreover, if the thermo-activated electron escape from QDs is induced by hot photoelectrons, this process reduces the relaxation losses, and improves PV efficiency.[14-16] Alternatively, the photoelectron capture from CB to QDs always decreases the light-induced shift of electron chemical potentials between CB and QDs, and in this way reduces V_{OC}. Therefore, the main requirement for improvement of the output voltage is not a suppression of thermo-activated escape from QDs with respect to the radiative transitions from QDs, but suppression of photoelectron capture to QDs with respect to the ban-to-band recombination. In the limit of strong suppression of capture, the QD-related increase in the short circuit current, δJ_{SC}, is expected to provide a small improvement in the open circuit voltage,

$$\delta V_{OC} = \frac{k_B T}{q} \frac{\delta J_{SC}}{J_{SC}}, \qquad (1)$$

where J_{SC} is the short circuit current in the device without QDs. Eq. 1 also assumes that the addition of QDs does not change recombination in the host material. Growth of QD media without defects that enhance recombination processes is a challenging technological problem. Finally, let us highlight that processes of electron escape and capture may by controlled by doping of the QD medium. The n-doping, i.e. negative charging of dots, increases thermo-activated escape, but reduces the photoelectron capture.

Nanoscale Accepted Manuscript

Kinetics of photoelectrons in structures with charged QDs has been intensively studied in QD IR photodetectors.[26-30] In particular, it was found that the n-charging of QDs exponentially suppresses the capture processes and exponentially increases IR photoresponse at liquid nitrogen temperatures.[29] Detailed studies of the potential barriers around dots[30] are useful for understanding why QD charging cannot efficiently suppress the photoelectron capture in traditional GaAs/InAs QD solar cells at room temperatures. First, due to relatively large phase volume of wetting layers (WLs) the capture processes from CB to dots are mainly occur via the WLs. The WLs play a role of shallow traps, so in the absence of QDs the WLs frequently capture electrons and return them to CB. In QD structures, the QDs mainly capture electrons that move in WLs. Second, the MBE-grown dots are strongly asymmetric with a low height-base aspect ratio. As a result, the potential barriers around dots in the direction of the QD plane are by an order in magnitude smaller than that in the direction perpendicular to the QD planes. Typical value for the in-plane barrier is 2-3 meV per electron localized in a QD [30] and, for example, five electrons per dot would substantially suppress the capture at nitrogen temperatures, but just slightly increase the capture time at room temperatures. Suppression of the WL-assisted capture to QDs at room temperatures would require very significant QD charging, which probably reduces the QD absorption. In this context, it is worth to highlight the original research[31] that demonstrates no degradation in the open circuit voltage in InAs/GaAs QD solar cells when compared to a solar cell grown without QDs and composed solely of WLs. This observation also evidences that capture processes via WLs may play a key role in V_{OC} reduction.

To formulate goals of this research, let us summarize the above discussion of processes in QD media. If QD levels create the IB, suppression of thermal extraction of electrons from QDs as well as suppression of electron relaxation to QDs are very challenging. The proposed suppression of the field-assisted thermal extraction from dots due to thick spacing layer[8,10,11] leads to localization of QD states and QD charging. The nanoscale barriers created via n-charging of QDs may be employed to suppress the photoelectron capture. However, suppression of the capture processes via WL would require very strong QD charging that decreases light harvesting by QDs. Therefore, reduction of wetting layer is expected to suppress photoelectron capture to QDs and to recover the open circuit voltage to that of the reference cell.

In this paper, we investigate GaAs solar cells with InAs QDs capped by AlGaAs layers, which practically eliminate WL states. We fabricated and characterized QD devices with WLs and with reduced wetting layers (RWL). A complete recovery of the open circuit voltage in the RWL QD devices with respect to the reference cell is shown.

II. Experimental

Two QD solar cell samples and a reference single junction GaAs sample were grown by molecular beam epitaxy using As_2 beam from a valved cracker source. Figure 1(a) shows cross section of the solar cell structures. The reference sample consists of 300 nm n^+-GaAs buffer layer and 50 nm n^+-$Al_{0.2}Ga_{0.8}As$ back surface field layer with doping

Nanoscale Accepted Manuscript

densities $5x10^{18}cm^{-3}$, 2.1 μm n-GaAs base layer doped to $2x10^{17}cm^{-3}$ with Si, 200 nm p-type emitter with carbon doping density of $5x10^{18}$ cm^{-3}. The entire stack was capped with a 30 nm p-$Al_{0.2}Ga_{0.8}As$ window with $5x10^{18}$ cm^{-3} doping and a 50 nm thick highly doped p^{+}-GaAs contact layer.

The two QDSC samples had a similar structure as that of the reference cell except that 1.1 μm thick QD stack was inserted in the base region next to the p-n junction. The QD stack consists of 20 layers of self-assembled InAs QDs separated by 50 nm GaAs spacers. The higher growth temperature and thickness of GaAs spacers were chosen to minimize defects formation and to suppress tunneling between the dots.

The QD section of the WL sample contained an 18 nm thick GaAs layer grown at 600^0C followed by 6 nm GaAs at 530^0C. The temperature was lowered for the growth of QD layer that consisted of 2 ML of InAs deposited on GaAs at 520^0C and capped with 5 nm GaAs at the same temperature, and further covered with 25 nm GaAs spacer layer at 600^0C. The RWL QD section consisted of 2.1 ML of InAs deposited on top of 7ML $Al_{0.2}Ga_{0.8}As$ barrier and capped with 2 ML of AlAs to suppress In surface redistribution and evaporation. The QD layer was covered with 7 ML of $Al_{0.2}Ga_{0.8}As$ barrier followed by deposition of 25 nm GaAs at 600^0C. The poor mobility of Al adatoms results in a conformal layer of AlAs on the quantum dots.[32-33] Therefore, besides reduction of the wetting layer this growth procedure also leads to formation of nanoscale AlGaAs barriers around InAs QDs.[34,35] Together with potential barriers, these barriers also enhance separation of localized QD states and CB.[34] Reduction of WL due to passivation of QDs with AlAs cap layer and its positive effect on V_{OC} were investigated in Ref. 36. Thus, the QD solar cells with reduced WLs demonstrate the better performance than traditional QD PV devices. However, the efficiency and V_{OC} of QD solar cells with reduced WLs were always below efficiency and V_{OC} of corresponding GaAs reference devices.[35,36] In our opinion, the decrease in efficiency is a consequence of the p-i-n structure of these QD devices. As we discussed in Introduction, placing of QD medium in the undoped region strongly enhances SRH recombination losses, but doping of QD medium with IB decreases efficiency due to charge accumulation at the boundaries of QD medium.

To evaluate the QD density, a partial solar cell structure with growth termination after completion of the fourth QD layer was capped with 2 ML of AlAs to prevent QDs from further evolution. The QD density measured with scanning electron microscopy (SEM) was close to $2x10^{10}$ cm^{-2}. Modulation doped QDs were prepared by placing 1nm Si-doped layers inside the GaAs spacers. The electrons from the dopant layer occupy the QDs ground states. The dopant sheet density was chosen to provide about one electron per dot. To observe the difference in the wetting layer formation and to verify the absence of strain-related dislocations, the QDSC structures were analyzed by cross-sectional transmission electron microscopy (TEM).

Square 300x300 μm^2 solar cells were fabricated using photolithography and dry etching for trench isolation down to the n-GaAs substrate. For p-type contact, a Cr/Au metal stack was deposited by electron beam evaporation followed by lift off. The samples were

Nanoscale Accepted Manuscript

passivated with silicon nitride (SiN) to minimize surface recombination. A blanket Indium metal layer was used as a backside contact.

Current-Voltage characteristics were measured under the Newport Oriel simulator at 1 Sun AM 1.5G (100 mW/cm^2) at room temperature. PMA 2100 pyranometer was used to calibrate the simulator intensity. Photoluminescence (PL) spectra were measured using 532 nm laser excitation, dispersed by a monochromator and detected using InGaAs photodetector. The external quantum efficiency spectral dependence was measured using halogen lamp and a monochromator as an optical source.

III. Results and Discussion

Transmission electron microscopy (TEM) studies of the QDSC samples were carried out to observe the details of the QD ensembles. Figure 1(b,c) shows cross-sectional dark field TEM micrographs obtained under g=200 diffraction conditions, where the structure factors predict InAs to appear bright and GaAs dark, while the strain contrast is less pronounced. The QDs in the WL sample are visibly larger than in the RWL sample; the image analysis gives the average lateral QD sizes of 21 nm and 16 nm, and QD sheet densities of 2x10^{10} cm^{-2} and 3x10^{10} cm^{-2} in the WL and RWL samples, respectively. The reduced QD size and increased density is related to dot nucleation on AlAs-containing surface.[32] In the WL sample image, the bright lines indicate formation of a thin wetting InAs layer almost everywhere between the dots. To observe the detailed structure of the wetting layer, high-angle annular dark field (HAADF) scanning TEM images are shown in Fig. 2 along with the intensity profiles averaged normal to the interfaces as indicated in the Figure. As HAADF image contrast is mostly sensitive to the atomic number (~z^2), the indium-containing atomic columns appear brighter with higher scattered intensity in the profiles, and the Al-containing layers have darker contrast (Figs. 2b,d). This property of HAADF imaging allows for direct visualization of In and Al distribution. The WL sample demonstrates quite wide (~9 MLs), brighter contrast corresponding to In segregation and surface redistribution during the QD overgrowth.[33,37] In the RWL sample, the InAs WL appears just 1.5-2ML thick which is due to fast "freezing" of the growing surface by deposition of 2ML AlAs. Small thickness of the InAs WL in the RWL sample along with the adjacent wide-bandgap AlAs capping likely results in pushing up the WL energy level to above the GaAs band edge[37] that is confirmed by the photoluminescence spectroscopy below. It is also noted that no dislocations were formed in the structure even though no strain-compensating layers were employed.

Luminescent properties of InAs/GaAs QDs with and without wetting layer were compared using room temperature photoluminescence (PL) measurements. Figure 3 shows PL spectra excited by 532 nm laser with intensity of ~20 W/cm^2. The ground state emission peaks were observed at 1030 nm and 1115 nm for the RWL and WL samples, respectively; the PL blue shift in the RWL sample is mainly due to reduction of QD sizes.[32] Based on the TEM results, the average numbers of atoms (In+As) in the QDs were estimated: 1.2x10^4 and 2.1x10^4 for the RWL and WL samples which predict the ground state transition wavelengths of 1055 nm and 1119 nm in InAs/GaAs QDs.[38] The match for the WL sample is good, and the extra ~20 meV redshift of the RWL peak

Nanoscale Accepted Manuscript

position can be explained by the additional AlSb wide-bandgap barrier layer affecting the quantum confinement energy.

The first excited state transitions appear as shoulders blue-shifted by ~63 meV from the ground state transition energies. The small peak observed for WL sample at 930 nm is related to the transitions in the InGaAs wetting layer, and these transitions are absent in the RWL sample. As discussed above, this likely results from high quantum confinement energy of carriers in a very thin InAs potential well embedded into a wider-bandgap AlGaAs (Fig. 2d) in the RWL sample. The stronger GaAs band-to-band recombination peak in the RWL sample evidences that the reduction of wetting layer strongly suppresses the capture processes, so the photocarriers mainly recombine via band-to-band processes.

Figure 4 shows current-voltage characteristics measured under 1 Sun AM 1.5G of the reference GaAs solar cell and two QDSC samples. Data from five devices measured across each wafer are presented to illustrate the variability of results. The parameters of the cells are summarized in Table I. Both QDSCs show a significant improvement of short circuit current (J_{SC}) as compared to the reference cell, but the open circuit voltage (V_{OC}) of the WL QDSC degrades by about 100 mV. Therefore, despite the 3 mA/cm^2 increase in short circuit current, the efficiency of the WL sample drops by 0.2% with respect to the reference GaAs cell. In contrast, the RWL sample with AlAs cap and $Al_{0.2}Ga_{0.8}As$ barriers maintained similar V_{OC} as the reference cell. The recovered open circuit voltage of the RWL sample is complemented by an additional 2.1 mA/cm^2 of J_{SC} and results in an absolute increase of 1.2% power conversion efficiency when compared to the reference sample.

Figure 5 shows dark I-V characteristics of the reference and two QDSC samples. First of all, let us note that the current of RWL sample is almost identical to that of the reference cell. To analyze generation-recombination processes around the open circuit voltage, we fitted the experimental dark current curves in the range 0.65 - 0.95 V by the two-diode model,

$$J_{dc}(V) = J_{01}\left(e^{\frac{q(V-I_{dc}R_{SR})}{k_BT}} - 1\right) + J_{02}\left(e^{\frac{q(V-I_{dc}R_{SR})}{2k_BT}} - 1\right), \qquad (2)$$

The first term in Eq. 2 is associated with the radiative G-R processes (ideality factor n = 1) and the second term with the Shockley–Read–Hall (SRH) recombination (n = 2) in the junction area. Two parameters J_{01} and J_{02} determined in this fitting procedure are presented in Table I. As seen, the J_{01} values are very close for RWL and Ref devices, while in the WL device the J_{01} increases by two orders in magnitude. This means that the radiative recombination is substantially enhanced in devices with WLs. In other words, WLs are effective traps that substantially enhances the radiative recombination processes. The J_{02} values are of the same order for all samples, which evidences that corresponding SRH recombination losses are close in all QD and reference cells. LeIt is worth noting that this is a result of significant doping of a QD medium with localized QD states. The doping reduces the width of the junction and decreases the SRH recombination losses in PV conversion. Contrary, in the IBSC design the QD medium is placed in the space

Nanoscale Accepted Manuscript

charge region with strong electric field and, therefore, the QD medium gives substantial SRH losses. The negative effect of the SRH recombination on V_{OC} is given by the dimensionless parameter $\zeta = J_{02}^2/(4J_{01}J_{OC})$, i.e. at $\zeta << 1$ the second term in Eq. 2 may be neglected. Calculations show that in this context the SRH recombination is negligible in WL devices. In the reference cell and QD RWL cell, the SRH the parameter ζ is 0.37 and 0.33 respectively, i.e. the SRH recombination in these devices is relatively small. Thus, in both reference cell and RWL device the V_{OC} is mainly determined by the radiative processes.

Figure 6 plots the comparison of external quantum efficiency spectra for the QDSC samples and the reference GaAs sample. The spectral response for all the samples resembles that of a typical GaAs SC with a band edge at 880 nm. Samples with QDs exhibit slightly higher response than the reference GaAs SC in the 700-880 nm band-to-band region. Relatively low absorption coefficient of GaAs in this region[39] (~10^4 cm^{-1}) makes the efficiency sensitive to the SC thickness in 1-3 μm range. In our QDSCs, the efficiency increase is due to either light scattering by QDs, or more likely due to the strong absorption of the above-GaAs-bandgap photons in the narrow-bandgap InAs QDs. This effect increases the photocurrent in the majority of the QDSC as shown in Table I. In the sub-bandgap range, the EQE of WL devices show the prominent peak at 930 nm, which corresponds to transitions to the wetting layer in agreement with the corresponding peak in the PL spectrum.

The contribution of the sub-bandgap radiation to the SC current was measured under 1 Sun (AM 1.5G) simulator with an IR longpass (λ>900 nm) filter. The photocurrents of 0.3 and 0.05mA/cm^2 were measured in the WL and RWL SCs, respectively. The ratio of these values (=6.0) is in a good agreement with the EQE data integrated over the sub-bandgap region (=7.2). It should be noted that EQE measurements were performed without optical bias; therefore, in both cases, the photocurrent was significantly less than under a sun simulator.

Now we consider the photocarrier kinetics in PV devices with localized intermediate states, obtain conditions for V_{OC} recovery, and discuss realization of these conditions in our measurements. For our goals it is convenient to present the Shockley-Queisser type kinetic equations for the photocarrier concentration in conduction band, n, and the concentration in QD states, n_1, in the following way

$$\frac{dn}{dt} = \frac{\dot{N}}{d} - \frac{n}{\tau_R} + \frac{\delta\dot{N}}{d} + \frac{n_1}{\tau_r} - \frac{n}{\tau_{cap}} + \frac{n_1}{\tau_{th}} , \quad (3)$$

$$\frac{dn_1}{dt} = \frac{\dot{N}_1}{d} - \frac{n_1}{\tau_{1R}} - \frac{n_1}{\tau_r} - + \frac{n_1}{\tau_{cap}} - \frac{n_1}{\tau_{th}} , \quad (4)$$

where d is the thickness of the absorber, $\dot{N}$ and $\dot{N}_1$ are the photon fluxes absorbed due to band-to-band transitions and transitions from the valence band to QD states

Nanoscale Accepted Manuscript

correspondingly, and $\delta\dot{N}$ is the addition to $\dot{N}$ due to enhancement of the band-to-band transitions by QDs, for example, due to photon scattering by QDs. The characteristic times describe the recombination, capture, and thermal generation: τ_R is the recombination time for carriers in the conduction band, τ_{1R} is the recombination time in QDs, τ_{cap} is the capture time to QDs, τ_{th} is the time of thermal escape from QDs to the conduction band, and τ_r is the characteristic time of the radiative transition from QDs to the conduction band. Let us take into account the detailed balance between capture and thermal escape processes in equilibrium,

$$n^{eq}/\tau_{cap} = n_1^{eq}/\tau_{th}, \tag{5}$$

and express the photocarrier concentrations via the photo-induced chemical potentials of carriers in the band, μ, and in QDs, μ_1,

$$\mu = k_B T \ln(n/n^{eq}), \ \mu_1 = k_B T \ln(n_1/n_1^{eq}). \tag{6}$$

Employing Eqs. 5 and 6, the kinetic equations (3) and (4) in stationary conditions take a form

$$\frac{\dot{N}}{d} - \frac{n^{eq}}{\tau_R}\exp\left(\frac{\mu}{k_B T}\right) + \frac{\delta\dot{N}}{d} + \frac{n_1^{eq}}{\tau_r}\exp\left(\frac{\mu_1}{k_B T}\right) - \frac{n^{eq}}{\tau_{cap}}\exp\left(\frac{\mu}{k_B T}\right)\left[1-\exp\left(\frac{\mu_1}{\mu}\right)\right] = 0 \tag{7}$$

$$\frac{\dot{N}_1}{d} - \frac{n_1}{\tau_{1R}}\exp\left(\frac{\mu_1}{k_b T}\right) - \frac{n_1^{eq}}{\tau_r}\exp\left(\frac{\mu_1}{k_b T}\right) + \frac{n^{eq}}{\tau_{cap}}\exp\left(\frac{\mu}{k_B T}\right)\left[1-\exp\left(\frac{\mu_1}{\mu}\right)\right] = 0. \tag{8}$$

Taking into account that $V_{OC} = \mu$, we can see that without QD medium the value of V_{OC} is determined by the two first terms in Eq. 7. The third and fourth terms in Eq. 7 describe small additions to the short circuit current due to QD enhanced band-to-band absorption (third) and contributions of two step absorption processes and hot-electron induced thermionic emission from QDs. The last term in Eqs. 7 and 8 describes the phonon-induced photocarrier exchange between the conduction band and QD localized states. If $\tau_{cap} << \tau_R$, the thermal exchange rate, $n^{eq}/\tau_{cap}\exp(\mu/k_B T)$, dominates over all other terms in Eqs. 7 and 8. Therefore, in this case, $\exp(\mu/\mu_1) = 1$, i.e. $\mu_1 = \mu$. Thus, under condition $\tau_{cap} << \tau_R$, the kinetic equations reduce to

$$\frac{\dot{N} + \dot{N}_1 + \delta\dot{N}}{d} - \left(\frac{n^{eq}}{\tau_R} + \frac{n_1^{eq}}{\tau_{1R}}\right)\exp\left(\frac{\mu}{k_B T}\right) = 0. \tag{9}$$

Eq. 9 has a form of the Shockley-Queisser equation for a single bandgap semiconductor with the bandgap value equal to the that in QDs. Thus, if the photoelectron capture to QDs dominates over the band-to-band radiative recombination, the addition of QD

Nanoscale Accepted Manuscript

medium to a single junction cell reduces V_{OC} and increases J_{SC}. Let us highlight that in this case the two-step absorption processes do not provide V_{OC} increase.

In the opposite case, $\tau_{cap} >> \tau_R$, the electron coupling between the conduction band and QDs is weak. Usually, QD media provides relatively small contribution to the short circuit current. Then the correction to V_{OC} may be calculated from Eqs. 7 and 8 in perturbative way,

$$\delta V_{OC} = \frac{k_B T}{q}\left(\frac{\delta J_{SC}}{J_{SC}} - \frac{\tau_R}{\tau_{cap}}\right), \tag{10}$$

where δJ_{SC} is the total increase in the short circuit current due to QD media. If the capture time goes to infinity, Eq. 10 is transformed into Eq. 1 that is obvious in the absence of the capture processes.

Now let us return to analysis of our experiments. According to the above discussion the condition for the voltage recovery is

$$\tau_{cap} \geq \tau_R . \tag{11}$$

The typical value of the band-to-band recombination time in GaAs is ~1 ns. It is well understood that in traditional InAs/GaAs QD structures the photoelectron capture is realized via WLs and the corresponding capture time is several picoseconds.[40,41] Thus, in QD media with WLs the capture time is by at least two orders of magnitude shorter than the recombination time and, therefore, the measured open circuit voltage is always substantially smaller than that in the reference cell.

In the QD structures without the wetting layer, the rate of photoelectron capture to the charged QD may be evaluated as[14,23,27]

$$\frac{1}{\tau_{cap}} \cong N_{QD} V_{QD} \frac{1}{\tau_\varepsilon} \exp\left(-\frac{q\varphi}{k_B T}\right), \tag{12}$$

where N_{QD} is the concentration of QDs, V_{QD} is the volume of a QD, φ is the average repulsive potential at QD boundary, which is proportional to the quantum dot charge, and τ_ε is the inelastic electron-phonon relaxation time, which corresponds to the transitions from the conduction band to relatively deep localized QD levels. It should be emphasized, that at low temperatures the capture to QDs has a cascade character. Firstly, an electron is trapped to delocalized QD states, such as minibands formed by periodically placed QD layers, and then relaxes to localized QD levels. At room temperatures electrons trapped to delocalized QD states are thermally excited back to the continuum states. Therefore, to be captured, electron should be directly trapped to relatively deep QD levels separated from the continuous spectrum by energy of at least 2 - 3 $k_B T$, which is typical value for electron level spacing in QDs. Such relaxation is realized via two-phonon emission, which may include various combinations of optical and acoustic modes. Detailed

Nanoscale Accepted Manuscript

calculations[42] show the two-phonon processes with transferred energy above 40 meV are very slow and the corresponding relaxation time exceeds 1 ns. However, defects strongly enhance the two-phonon relaxation and reduce the relaxation time, τ_ε , to several picoseconds.[43] Taking into account that in our QD media $N_{QD}V_{QD} = 0.02$ and for one-electron QD charging the exponential factor is 0.3, from Eq. 12 we obtain the capture time of ~1 ns. Thus, the capture time significantly increases in QD media with suppressed WL and even for one-electron charging has the same order as the recombination time. As discussed, the voltage recovery takes place when τ_{cap} reaches τ_R .

IV. Conclusions

Engineering of nanoscale potential profile is an effective tool to control electron processes in solar cells. We fabricated and studied photovoltaic devices with various QD media. EQE measurements and direct measurements with IR longpass filter under 1 Sun show that harvesting of sub-bandgap photons in QD media provides 0.3 mA/cm^2 and 0.05 mA/cm^2 contributions in the WL and RWL devices, respectively. The EQE and photovoltaic measurements with and without optical/IR bias show that in our devices the light-induced two-step transitions provide relatively small contribution to photovoltaic conversion. Thus, we confirm[8-11,13] that thermal excitation processes mainly determine electron transitions from QDs to CB. However, thermal excitation from QDs does not reduce the short circuit voltage with respect to the reference cell. Our main result is complete voltage recovery in QD devices with reduced wetting layer. The recovery has been reached due to suppression of electron capture processes from CB to QDs. Reduction of the WL and n-charging of QDs strongly prevent capture of photoelectrons and, therefore, maintain the light-induced shift between chemical potentials of electrons in QDs and the CB.

Let us note that the highest values of V_{OC} (0.994 V) in a QD solar cell close to the reference cell V_{OC} (1.04 V) were observed in Ref. 9. However, these devices were designed as p-i-n structures, where very thin (100 nm) i-region in the reference device was replaced in QD cell by the ten layer QD medium of approximately the same thickness. Therefore, in all these structures the light-induced chemical potential was mainly generated in the thick (~3 μm) n-doped region, while the contribution of the 100nm i-region (QD medium) was small due to its small relative thickness.

The presented description of photoelectron processes and their contributions to photovoltaic conversion also provide qualitative explanation of the recent results by other groups. To the best of our knowledge, the voltage recovery was studied in QD PV devices with relatively thick spacer layers (> 30 nm), i.e. in devices with localized QD states. Therefore, it is not surprising that the obtained results show strong dependence of the open circuit voltage on the QD charge and its significant improvement due to n-doping. Ref. 18 reported the voltage recovery of 121 mV that was observed in the sample with the eight electrons per dot compared with the undoped sample. Recent work[19] studied the QD in well structures and reported 105 mV voltage recovery at the doping level of eighteen electrons per dot. As we discussed in the Introduction, the n-doping of QD media reduces electron capture to QDs, but enhances the electron thermal

Nanoscale Accepted Manuscript

escape from QDs. Thus, the voltage recovery requires significant suppression of the capture processes with respect to the band-to-band recombination, but not thermal escape from QDs with respect to corresponding radiative transition.

Despite some voltage recovery due to n-doping,[18,19] in all papers the V_{OC} of QD devices was found to be below that of the reference cells. The complete voltage recovery was only demonstrated in the doped QD structures with thick spacer (80 nm) at low temperatures.[21,22] Taking into account that carrier capture is mainly realized via emission of optical phonon,[27-29] strong suppression of the carrier capture to QDs at low temperatures is highly expected. Thus, the results of Refs. 21 and 22 also show that the photoelectron capture is main reason for the V_{OC} reduction.

Control of nanoscale physical processes that strongly affect the open circuit voltage is important for development of various QD photovoltaic materials and devices. Nanomaterials with charged QDs and corresponding 3D nanoscale potential profile provide real mechanisms for suppression of photoelectron capture and increasing the output voltage.

Acknowledgements

This research was supported by the National Science Foundation under grant ECS-1236459. AS acknowledges support by NRC.

References

[1] A. Green, *Third Generation Photovoltaics*, Springer, Berlin Heidelberg New York, 2003.

[2] H. A. Atwater and A. Polman, *Nature Materials*, 2010, 9, 205-213.

[3] K. Ladutenko, P. Belov, O. Peña-Rodríguez, A. Mirzaei, A. E. Miroshnichenko, and I. V. Shadrivov, *Nanoscale,* 2015, advance article.

[4] R. D. Schaller and V. I. Klimov, *Phys. Rev. Lett.,* 2004, 92, 186601.

[5] R. J. Ellingson, M. C. Beard , J. C. Johnson et al., *Nano Lett.,* 2005, 5, 865-871.

[6] XL. Zhang, JH. Liu, E. M. J. Johansson, EMJ Johansson, *Nanoscale,* 2015, 7, 1454-1462.

[7] A. Luque, A. Marti, *Phys. Rev. Lett.*, 1997, 78, 5014.

[8] E. Antolín, A. Martí, C. D. Farmer et al., *App. Phys. Lett*., 2010, 108, 064513.

[9] C. G. Bailey, D. V. Forbes, R. P. Raffaelle, and S. M. Hubbard, Appl. Phys. Lett., 2011, 98, 163105.

[10] S. Asahi, H. Teranishi, N. Kasamatsu et al., *J. Appl. Phys.*, 2014, 116, 063510.

[11] D. G. Sellers, S. Polly, S. M. Hubbard, and M. F. Doty, *Appl. Phys. Lett.*, 2014, 104, 223903.

[12] M. Usman, *Nanoscale*, 2015, 7, 16516-16529.

Nanoscale Accepted Manuscript

[13] Y. Okada, N. J. Ekins-Daukes, T. Kita et al., *Appl. Phys. Rev.*, 2015, 2, 021302.

[14] K.A. Sablon and A. Sergeev, *Emerging PV Nanomaterials: Capabilities versus Recombination Losses*, in: Xiaodong Wang and Zhiming M. Wang (eds), *High-Efficiency Solar Cells: Physics, Materials, and Devices*, Springer Series in Materials Science, V. 190, 2014, pp. 85-114.

[15] K. Sablon, J. Little, N. Vagidov et al., *Appl. Phys. Lett.*, 2014, 104, 253904.

[16] D. Watanabe, N. Kasamatsu, Y. Harada, and T. Kita, *Appl. Phys. Lett.*, 2014, 105, 171904.

[17] S. Oktyabrsky, M. Lamberti, V. Tokranov, G. Agnello and M. Yakimov, J. Appl. Phys. 98, 053512 (2005).

[18] S. J. Polly, D. V. Forbes, K. Driscoll, S. Hellstrom, and S. M. Hubbard, *IEEE J. Photovoltaics*, 2014*,* 4, 1079-1085.

[19] P. Lam, S. Hatch, J. Wu, M. Tang, V. G. Dorogan, Yu. Mazur, G. J. Salamo, I. Ramiro, A. Seeds, H. Liu, *Nano Energy*,2014, 6, 159-166.

[20] T. Tayagaki, Y. Hoshi, and N. Usami, *Scientific Reports*, 2013, 3, 2703.

[21] P. G. Linares, A. Martı, E. Antolın, C. D. Farmer, I. Ramiro, C. R. Stanley, and A. Luque, *Solar Energy Materials and Solar Cells*, 2012, 98, 240-244.

[22] P. G. Linares, A. Martı, E. Antolın, C. D. Farmer, I. Ramiro E. Lopez, E. Hernandez, D. F. Marron, I. Artacho, I. Tobıas, P. Gerard, C. Chaix, R. P. Campion, C. T. Foxon, C. R. Stanley, S. I .Molina, and A. Luque, *Solar Energy Materials and Solar Cells*, 2013, 108, 175-179.

[23] K. A. Sablon, J. W. Little, V. Mitin, A. Sergeev, N. Vagidov, and K. Reinhardt, *Nano Letters*, 2011, 11, 2311-2317.

[24] K. A Sablon, A. Sergeev, N. Vagidov, J. W. Little, and V. Mitin, *Solar Energy Materials and Solar Cells*, 2013, 117, 638-644.

[25] K. Sablon, Y. Li, N. Vagidov, V. Mitin, J. W. Little, H. Hier, and A. Sergeev, *Appl. Phys. Lett.*, 2015, 107, 073901.

[26] V. Ryzhii, *Semiconductor Science and Technology*, 1996, 11, 759-765.

[27] A. Sergeev, V. Mitin, and M. Stroscio, *Physica B*, 2002, 316-317, 369-372.

[28] V. Mitin, A. Sergeev, N. Vagidov, and S. Birner, *Infrared Physics & Technology*, 2013, 59, 84-88.

[29] V. Mitin, A. Antipov, A. Sergeev, N. Vagidov, D. Eason, and G. Strasser, *Nanoscale Res. Lett.*, 2011, 6, 21.

[30] K. Sablon, A. Sergeev, N. Vagidov, A. Antipov, J.W. Little, and V. Mitin, *Nanoscale Res. Lett.*, 2011, 6, 584.

[31] D. Guimard, R. Morihara, D. Bordel, K. Tanabe, Y. Wakayam, M. Nishioka, Y.A. Arakawa, *Appl. Phys. Lett.*, 2010, 96, 203507.

Nanoscale Accepted Manuscript

[32] G. Agnello, V. Tokranov, M. Yakimov, M. Lamberti, Y. Zheng, and S. Oktyabrsky *Proc. MRS.*, 2004, 829, B2.1-6.

[33] S. Oktyabrsky, V. Tokranov, G. Angello, J. van Eisden, and M. Yakimov, *J. Electron. Mater.*, 2006, 35, 822.

[34] G. Wei and S. R. Forrest, *Nano Letters*, 2007, 7, 218-222.

[35] K. A. Sablon, J. W. Little, K. A. Olver, Zh. M. Wang, V. G. Dorogan, Yu. I. Mazur, G. J. Salamo, and F. J. Towner, *J. Appl. Phys.*, 2010, 108, 074305.

[36] F. K. Tutu, P. Lam, J. Wu, N. Miyashita, Y. Okada, K.-H. Lee, N. J. Ekins-Daukes, J. Wilson, and H. Liu, *Appl. Phys. Lett.*, 2013, 102, 163907.

[37] M. Yakimov, V. Tokranov, G. Agnello, J. van Eisden, and S. Oktyabrsky, *J. Vac. Sci. Tech.*, 2005, B 23, 1221.

[38] C. Pryor, *Phys Rev. B*, 1999, 60, 2869-2874.

[39] H. C. Casey , D. D. Sell , and K. W. Wecht , *J. Appl. Phys.*, 1975, 46, 250.

[40] R. Heitz, M. Veit, N. N. Ledentsov, A. Hoffmann, D. Bimberg, V. M. Ustinov, P. S. Kop'ev, and Zh. I. Alferov, *Phys. Rev. B*, 1997, 56, 10435.

[41] T. Muller, F. F. Schrey, G. Strasser, and K. Unterrainer, *Phys. Rev. B*, 2003, 83, 3572.

[42] T. Inoshita and H. Sakaki, *Phys. Rev. B,* 1992, 46, 7260-7263.

[43] A. N. Poddubny and S. V. Goupalov, *Phys. Rev. B*, 2008, 77, 075315.

Nanoscale Accepted Manuscript

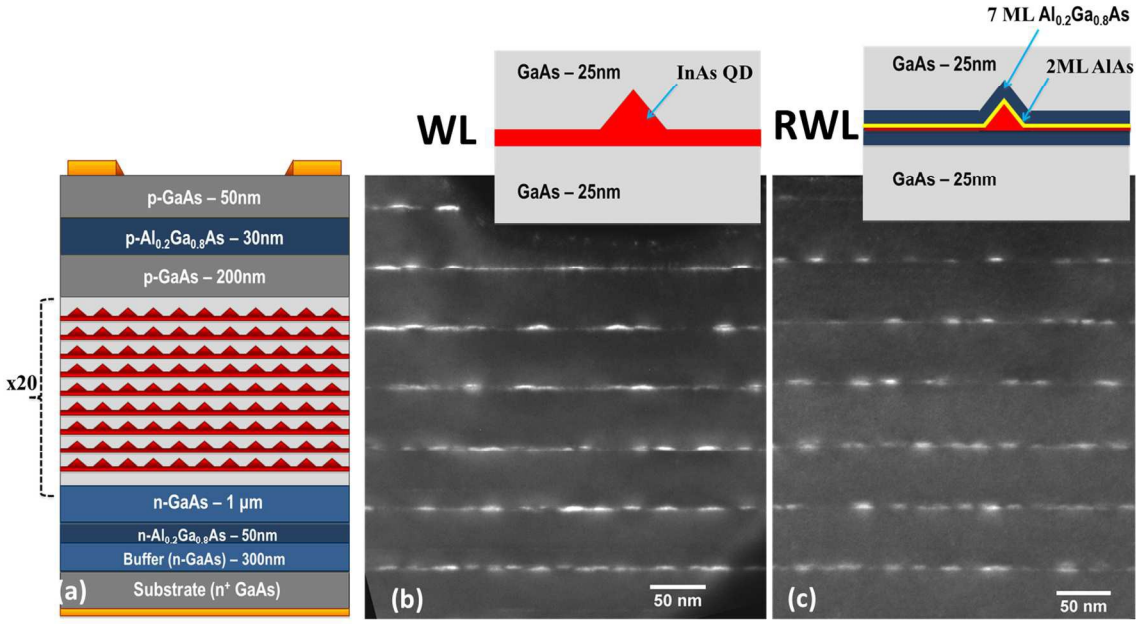

FIG.1. (a) Schematic of a QD solar cell structure grown on n-GaAs (001) substrate with 20 layers (1.1 μm thick) of InAs QDs. (b-c) Dark field g = (002) micrographs of the QD structures (b) with wetting layer (WL) and (c) with a reduced wetting layer (RWL). Insets: detailed structures of the WL and RWL QD samples.

Nanoscale Accepted Manuscript

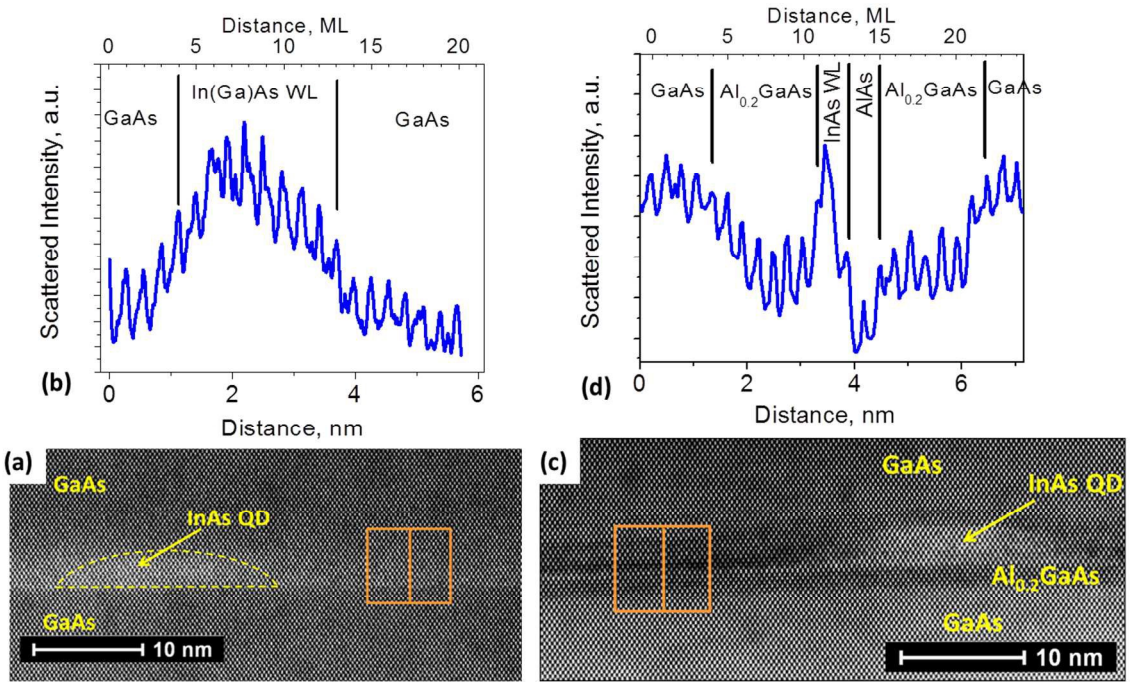

FIG.2. High-angle annular dark field scanning TEM images of (a) WL and (c) RWL samples with corresponding high-resolution intensity profile across the wetting layer regions in (b) and (d), respectively. Intensity oscillations correspond to atomic columns.

Nanoscale Accepted Manuscript

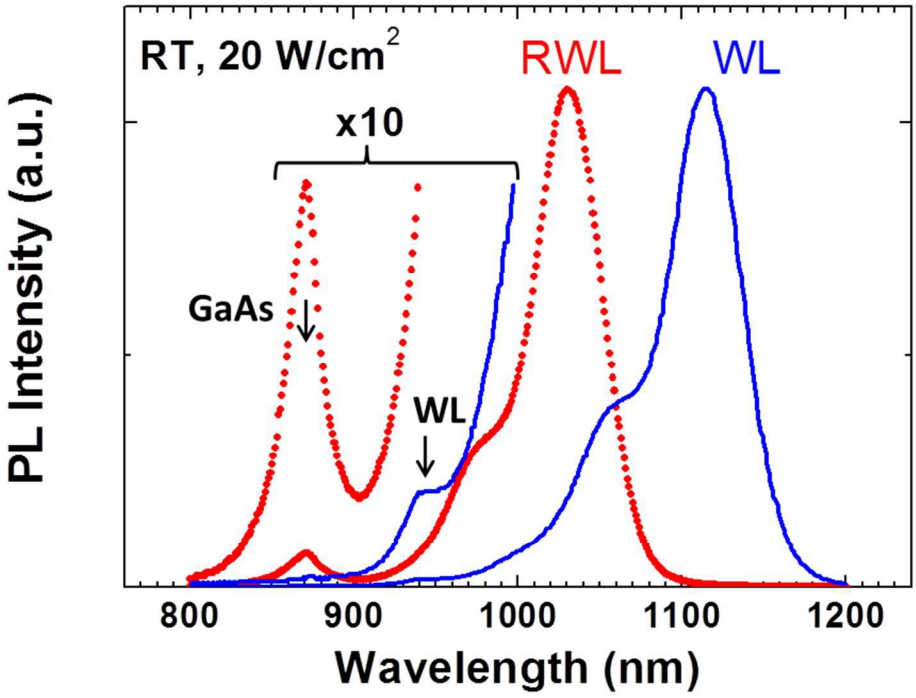

FIG.3. Photoluminescence spectra for quantum dot solar cell samples measured at room temperature. Excitation intensity is ~20W/cm^2 at 532nm.

Nanoscale Accepted Manuscript

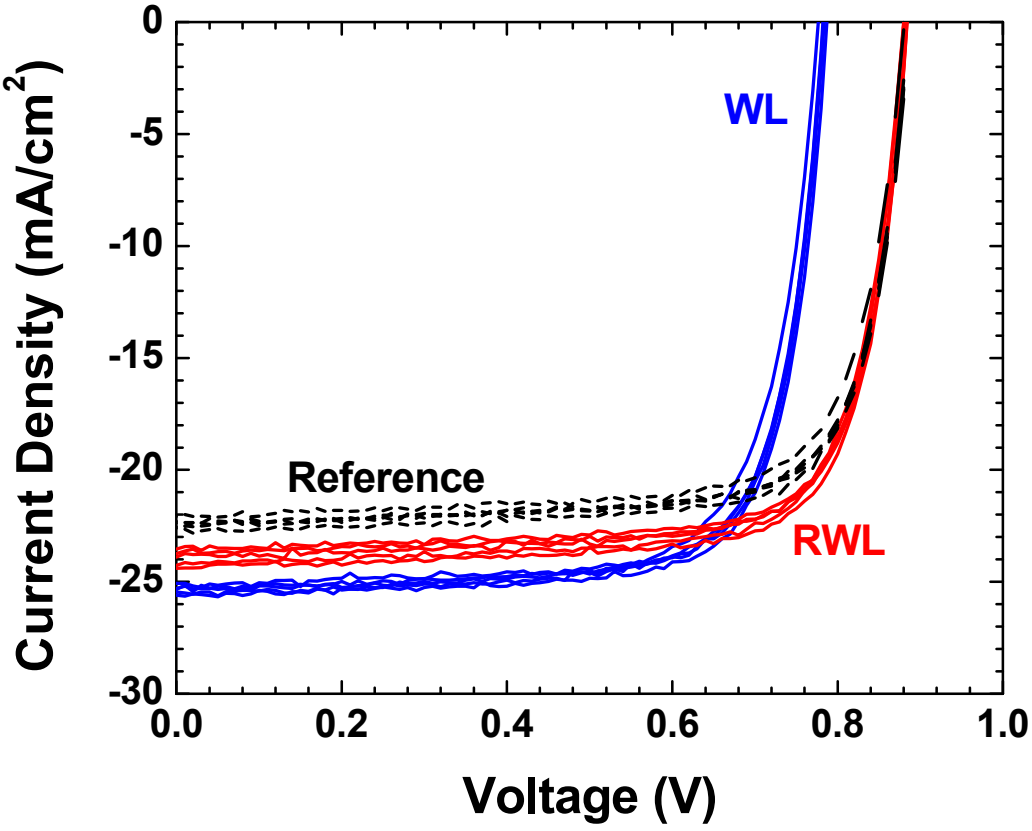

FIG.4. Current – voltage characteristics of a reference GaAs and two QDSC samples under 1 Sun (AM 1.5G) illumination. Data from five devices from each wafer are shown.

Nanoscale Accepted Manuscript

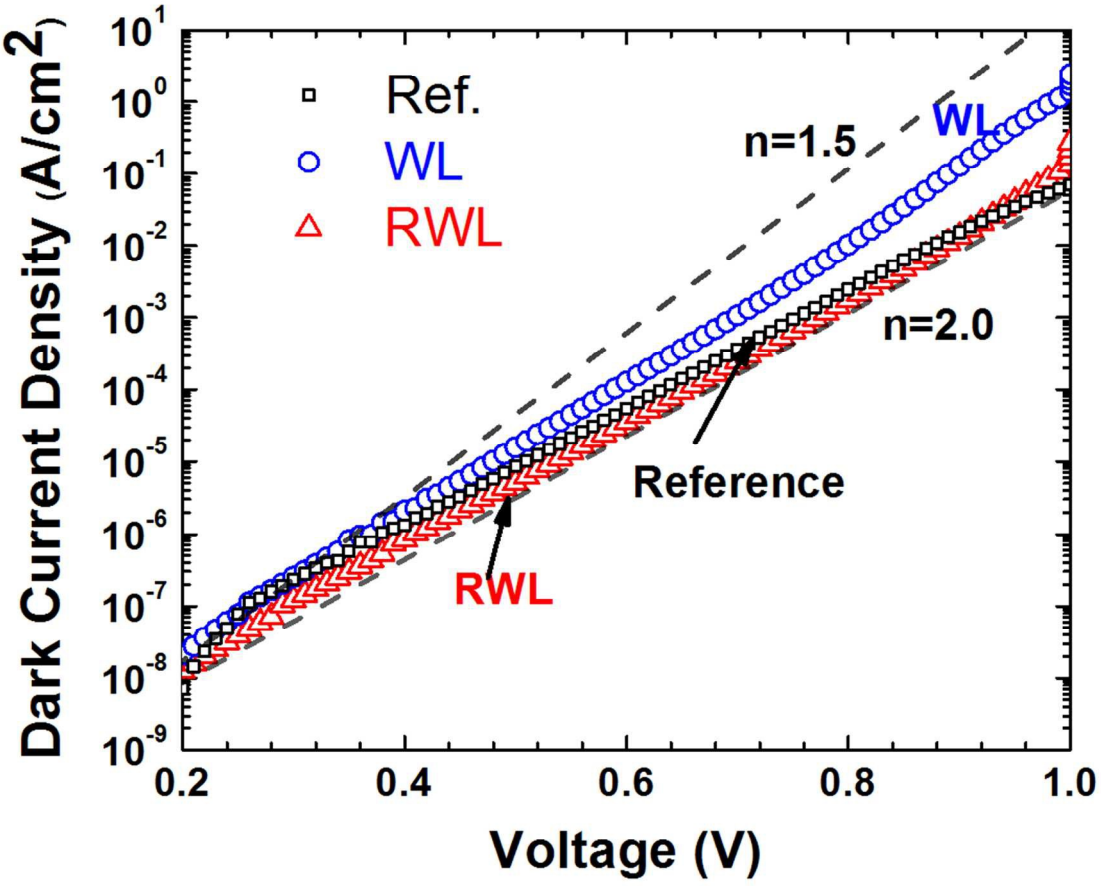

FIG.5. Dark current – voltage characteristics of the reference GaAs sample and the two QDSC samples. Dashed lines indicate the exponents with ideality factors 1.5 and 2.0.

Nanoscale Accepted Manuscript

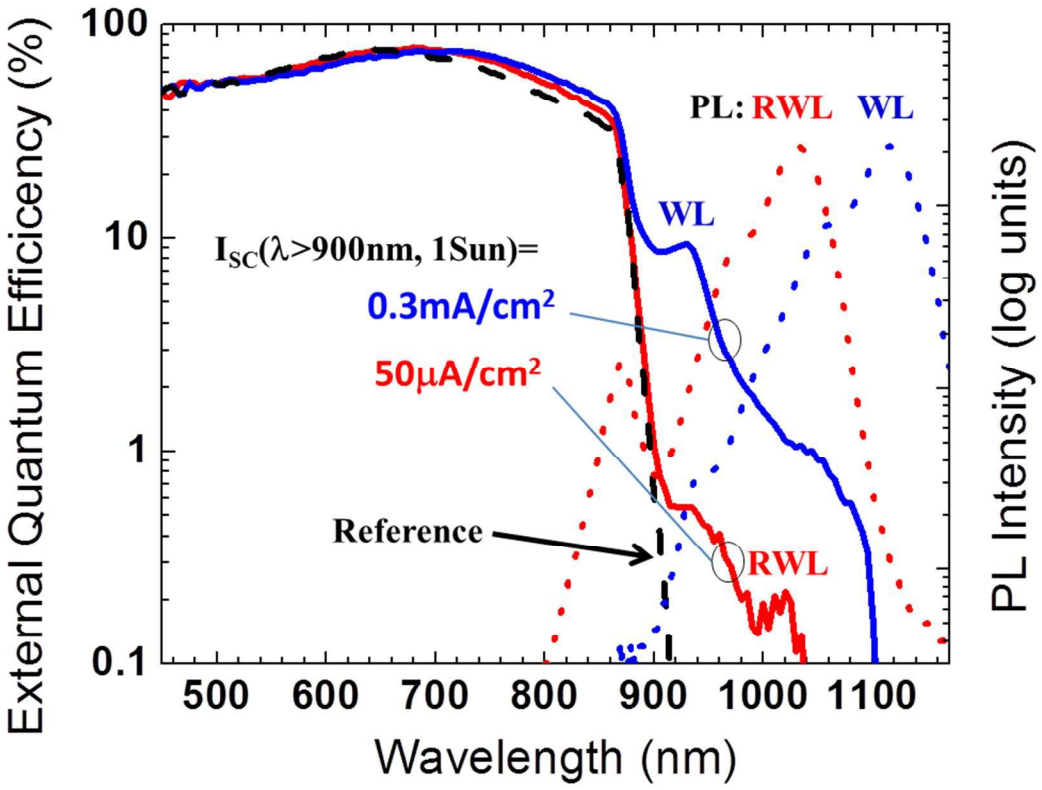

FIG.6. EQE spectra of reference GaAs and two QDSCs showing bulk GaAs and sub-bandgap absorption regions. The integrated sub-bandgap short circuit current is measured under 1 Sun simulator with an IR longpass (λ>900 nm) filter. Dotted lines show PL spectra of QD samples as in Fig. 3 in logarithmic scale.

Nanoscale Accepted Manuscript

Table I: Measured open circuit voltage (V_{OC}), short circuit current density (J_{SC}), fill factor (FF), efficiency (η), short circuit current with longpass filter for reference GaAs and QDSC samples under 1 Sun AM 1.5G simulator, and the J_{01} and J_{02} components of the dark current density in two-diode model fitting.

Sample	J_{SC} (mA/cm^2)	V_{OC} (V)	FF	Efficiency (%)	J_{SC}(>900nm) (mA/cm^2)	J_{01} (A/cm^2)	J_{02} (A/cm^2)
Ref.GaAs	22.6	0.88	77	15.4	0	2.7×10^{-18}	3.0×10^{-10}
WL	25.6	0.78	76	15.2	0.3	6.0×10^{-16}	9.0×10^{-10}
RWL	24.7	0.88	76	16.6	0.05	3.1×10^{-18}	3.2×10^{-10}

Nanoscale Accepted Manuscript